

Causal-SAM-LLM: Large Language Models as Causal Reasoners for Robust Medical Segmentation

Tao Tang¹, Shijie Xu², Yiting Wu², and Zhixiang Lu^{*2}

¹ City University of Hong Kong, Hong Kong, China

² Xi'an Jiaotong-liverpool University, Suzhou, China
Zhixiang@liverpool.ac.uk

Abstract. The clinical utility of deep learning models for medical image segmentation is severely constrained by their inability to generalize to unseen domains. This failure is often rooted in the models learning spurious correlations between anatomical content and domain-specific imaging styles. To overcome this fundamental challenge, we introduce **Causal-SAM-LLM**, a novel framework that elevates Large Language Models (LLMs) to the role of causal reasoners. Our framework, built upon a frozen Segment Anything Model (SAM) encoder, incorporates two synergistic innovations. First, **Linguistic Adversarial Disentanglement (LAD)** employs a Vision-Language Model to generate rich, textual descriptions of confounding image styles. By training the segmentation model's features to be contrastively dissimilar to these style descriptions, it learns a representation robustly purged of non-causal information. Second, **Test-Time Causal Intervention (TCI)** provides an interactive mechanism where an LLM interprets a clinician's natural language command to modulate the segmentation decoder's features in real-time, enabling targeted error correction. We conduct an extensive empirical evaluation on a composite benchmark from four public datasets (BTCV, CHAOS, AMOS, BraTS), assessing generalization under cross-scanner, cross-modality, and cross-anatomy settings. Causal-SAM-LLM establishes a new state of the art in out-of-distribution (OOD) robustness, improving the average Dice score by up to **6.2 points** and reducing the Hausdorff Distance by **15.8 mm** over the strongest baseline, all while using less than 9% of the full model's trainable parameters. Our work charts a new course for building robust, efficient, and interactively controllable medical AI systems.

Keywords: Domain Generalization · Large Language Models · Medical Image Segmentation · Causal Inference · Multi-Modal Information Processing.

* Corresponding author.

1 Introduction

Deep learning models, especially those based on foundational architectures like U-Net [1] and the Segment Anything Model (SAM) [2], have demonstrated remarkable proficiency in medical image segmentation. Yet, a critical chasm persists between their performance in controlled academic settings and their reliability in real-world clinical environments. This “lab-to-clinic” gap is primarily due to a lack of robustness; a model trained on data from one hospital’s CT scanner often exhibits a precipitous performance drop when deployed on images from another hospital’s MRI machine [3,4]. This brittleness arises because models exploit spurious correlations, mistaking domain-specific imaging style for the anatomical content [5].

The advent of Vision Foundation Models (VFMs), pre-trained on internet-scale data, offered a promising path forward, as their feature spaces are believed to implicitly disentangle content from style. However, the very process of adapting these powerful models proves to be their Achilles’ heel. Fine-tuning even with parameter-efficient methods like LoRA [6] can cause catastrophic forgetting or, more subtly, a “re-entanglement” of features, forcing the model to re-learn the spurious correlations present in the smaller, domain-specific medical dataset. This motivates our central research question: “Can we harness the abstract reasoning capabilities of Large Language Models to enforce causal invariance in vision models during training and facilitate interactive, user-guided error correction during inference?”

We introduce **Causal-SAM-LLM** as a comprehensive answer. Our framework posits a novel synergy: leveraging the high-level, semantic reasoning of LLMs to govern the low-level feature representations of vision models. It uniquely integrates LLM-driven intelligence into the segmentation pipeline at two critical junctures:

1. **During Training:** We propose a **Linguistic Adversarial Disentanglement (LAD)**. Recognizing that imaging style is not a monolithic category but a rich spectrum of visual attributes, we use a pre-trained Vision-Language Model (VLM) [7] to generate detailed textual descriptions of an image’s style (e.g., “low-contrast T2-weighted MRI with significant motion artifact and signal inhomogeneity”). By enforcing a contrastive loss that pushes the model’s visual features away from the embedding of this text, we compel the model to learn what to ignore on a fine-grained, semantic level.
2. **During Inference:** We introduce **Test-Time Causal Intervention (TCI)**. An LLM-based Causal Reasoner module interprets natural language commands from a user, such as a radiologist observing an error. The LLM translates this command into modulation parameters for FiLM layers [8] integrated within the segmentation decoder, enabling precise, on-the-fly correction. This elevates the model from a static predictor to a dynamic, collaborative reasoning system.

Our contributions are four-fold:

1. We establish a new paradigm for robust medical segmentation where LLMs act as explicit causal reasoners to guide and control a vision model, a departure from their traditional use in generation or captioning tasks.
2. We introduce LAD, a new training objective that leverages the semantic richness of VLM-generated text to purge complex, fine-grained style confounders from the model’s feature space.
3. We operationalize a TCI mechanism, enabling real-time, user-driven model adaptation through natural language, a significant step towards practical and trustworthy clinical AI.
4. We conduct extensive empirical validation on a challenging benchmark of four public datasets, setting a new state-of-the-art in out-of-distribution performance across cross-scanner, cross-modality, and cross-anatomy generalization scenarios.

2 Related Work

2.1 Foundation Models in Medical Imaging

The advent of Vision Foundation Models (VFM) like SAM [2] and its medical variants [9] has reshaped image analysis. Adapting these powerful, generalist models to specialized medical tasks is a primary challenge. The main strategies are full fine-tuning, which risks catastrophic forgetting and overfitting by updating all parameters (θ), and Parameter-Efficient Fine-Tuning (PEFT), the now-dominant paradigm. PEFT methods like LoRA [6] freeze the large VFM backbone (θ_{frozen}) and optimize only a small set of new parameters (ϕ), where $|\phi| \ll |\theta_{\text{frozen}}|$. For instance, LoRA constrains a weight update ΔW with a low-rank decomposition, $W' = W_0 + BA$, making the optimization computationally feasible:

$$\phi^* = \arg \min_{\phi} \mathcal{L}(\mathcal{M}_{\theta_{\text{frozen}}, \phi}(X), Y)$$

However, both full fine-tuning and PEFT share a fundamental limitation: their objective is task adaptation, not causal robustness. Because they are optimized to fit the source data distribution, they invariably learn the spurious correlations present within it. This leaves them inherently vulnerable to failure when deployed on out-of-distribution (OOD) data where these correlations do not hold.

To solve this, we propose a new paradigm that decouples perception from causal reasoning. We treat the VFM as a fixed, powerful feature extractor, $f_{\theta_{\text{VFM}}}$, whose pristine representations are never corrupted by fine-tuning. We then build a lightweight, external causal reasoning system, g_{ψ} , on top of it, confining the optimization entirely to our proposed modules:

$$\psi^* = \arg \min_{\psi} \mathcal{L}(g_{\psi}(f_{\theta_{\text{VFM}}}(X)), Y)$$

This approach fully preserves the VFM’s generalizable knowledge and shifts the learning objective from mere “weight adaptation” to explicit “behavioral guid-

ance.” Our framework is therefore orthogonal to PEFT and directly addresses the critical, unsolved challenge of causal robustness in medical segmentation.

2.2 Domain Generalization and Adaptation

The goal of Domain Generalization (DG) is to learn a model on source domains $\{(\mathcal{D}_{S_i})\}_{i=1}^N$ that minimizes the risk on an unseen target domain \mathcal{D}_T . Key paradigms include:

Distribution Alignment. These methods learn domain-invariant features by minimizing the discrepancy between domain distributions. This can be done adversarially, as in Domain-Adversarial Neural Networks (DANN) [10], which use a domain classifier \mathcal{D}_c in a minimax game against a feature extractor \mathcal{E}_f :

$$\min_{\mathcal{E}_f, \mathcal{C}_y} \max_{\mathcal{D}_c} \mathcal{L}_{task} - \lambda \mathcal{L}_{domain}(\mathcal{D}_c(\mathcal{E}_f(x)), d)$$

Alternatively, methods can directly minimize statistical distances like MMD [11] or CORAL [12], which aligns feature covariance matrices (C_S, C_T) :

$$\mathcal{L}_{CORAL} = \frac{1}{4d^2} \|C_S - C_T\|_F^2$$

The core limitation is the assumption that aligning low-order statistics is a sufficient proxy for semantic invariance.

Data and Feature Augmentation. A parallel approach is to synthesize a wider variety of styles during training. MixStyle [13], inspired by style transfer [14], creates novel feature statistics by linearly interpolating the channel-wise mean and standard deviation of instance pairs:

$$\tilde{\mathbf{z}}_i = (\lambda\sigma_j + (1-\lambda)\sigma_i) \frac{\mathbf{z}_i - \mu_i}{\sigma_i} + (\lambda\mu_j + (1-\lambda)\mu_i)$$

This encourages robustness by training the model on a synthesized spectrum of styles.

Test-Time Adaptation (TTA). TTA adapts a source-trained model to unlabeled test data. Methods like TENT [15] achieve this by updating only the Batch Normalization parameters (γ, β) to minimize the entropy of the model’s predictions on the test batch:

$$\min_{\gamma, \beta} \mathcal{H}(\text{Softmax}(\mathcal{M}(x_t)))$$

Causal Perspective. From a causal viewpoint, these methods treat the domain as a statistical confounder but lack a semantic understanding of it. They attempt to neutralize its effect via statistical alignment, data diversification, or unsupervised self-correction. This risks discarding valuable features or failing to address specific, nuanced artifacts. Our framework offers a more surgical alternative. Instead of inferring confounders statistically, our **Linguistic Adversary** uses language to explicitly *name* them, enabling a precise semantic disentanglement. Furthermore, our **Test-Time Intervention** replaces unsupervised, entropy-driven adaptation with knowledge-driven causal interventions guided by human reason. This elevates the approach from statistical pattern matching to explicit causal reasoning.

2.3 Causality and Disentanglement in Vision

Applying the formalisms of causality [16] to build robust AI systems is a critical research frontier. The goal is to learn models that understand the true data-generating process, often conceptualized as a Structural Causal Model (SCM), where each variable X_i is a function of its parents PA_i and an independent noise term U_i , i.e., $X_i := f_i(PA_i, U_i)$. However, defining a complete SCM for high-dimensional image data is often intractable.

Consequently, research has focused on proxies for causality. One direction is learning disentangled representations, where latent factors of variation are separated into semantically meaningful axes [17]. The assumption is that these axes correspond to independent causal variables. This often requires strong inductive biases, such as the objective in β -VAE, which penalizes latent complexity:

$$\mathcal{L}_{\beta\text{-VAE}} = \mathbb{E}_{q(\mathbf{z}|\mathbf{x})}[\log p(\mathbf{x}|\mathbf{z})] - \beta D_{KL}(q(\mathbf{z}|\mathbf{x})\|p(\mathbf{z}))$$

Despite this, purely unsupervised disentanglement without such biases remains theoretically impossible [18]. Another major direction is invariant learning. Methods like Invariant Risk Minimization (IRM) [19] seek a representation Φ that enables a single classifier w to be simultaneously optimal across all training environments $e \in \mathcal{E}_{tr}$. The formal objective is:

$$\min_{\Phi: \mathcal{X} \rightarrow \mathcal{H}} \sum_{e \in \mathcal{E}_{tr}} R^e(\Phi) \quad \text{s.t.} \quad w \in \arg \min_{w'} R^e(w' \circ \Phi)$$

The hypothesis is that an invariant representation Φ captures the true causal mechanism. However, these methods require access to diverse training environments and attempt to infer invariance from statistical regularities alone.

Our work circumvents the limitations of these statistical approaches. Instead of tasking the model with the difficult problem of unsupervised causal discovery, we use a VLM to explicitly name the confounder. This linguistic grounding enables a precise, supervised causal intervention, providing the explicit knowledge that methods like IRM attempt to infer implicitly.

2.4 Interactive Segmentation and LLMs in Medicine

Recent language-guided interactive segmentation has focused on a declarative paradigm, where text specifies what to segment. Models like LISA [20] and SEEM [21] excel at this, mapping an image I and a target prompt p_{target} to a segmentation mask M :

$$M = f(I, p_{\text{target}})$$

In this role, language acts as a semantic pointer, an input to the function. While powerful, these frameworks are not designed to modify their internal segmentation logic based on corrective feedback.

In contrast, our work defines a complementary, interventional paradigm where language is used to correct the segmentation process. A user prompt such as “ignore the motion artifact” does not change the segmentation target but executes a causal intervention on the model’s behavior. Formally, given an initial model f_{θ} and a corrective prompt $p_{\text{corrective}}$, our framework produces a modulated model $f_{\theta'}$ to generate the final mask M' :

$$M' = f_{\theta'}(I), \quad \text{where} \quad \theta' = g(\theta, p_{\text{corrective}})$$

This distinction is fundamental. We repurpose language from an input that defines a target to a control knob that modulates the function itself ($\theta \rightarrow \theta'$). This capability to perform knowledge-driven, on-the-fly causal intervention for quality control is a key contribution not addressed by prior interactive or VLM frameworks.

3 Methodology

Our framework, shown in Figure 1, is architected around a frozen vision encoder, \mathcal{E}_{SAM} (from ViT-H [22]), which extracts a feature representation $\mathbf{f} \in \mathbb{R}^d$ from an input image $\mathbf{x} \in \mathbb{R}^{H \times W \times C}$. The innovation is concentrated in the lightweight, trainable modules that leverage LLM intelligence to process \mathbf{f} .

3.1 Linguistic Adversarial Disentanglement

To achieve a semantically rich disentanglement, we use a frozen medical VLM, \mathcal{E}_{VLM} (specifically, LLaVA-Med [7]), to generate a textual description of an image’s style attributes: $t_{\text{style}} = \mathcal{E}_{VLM}(\mathbf{x})$.

Our objective is to render the image features \mathbf{f} semantically orthogonal to the style description t_{style} , making them uninformative about the image’s domain-specific properties. We frame this as a contrastive learning problem where we explicitly penalize any correlation between the image representation and the textual style embedding.

First, we leverage a pre-trained and frozen CLIP text encoder, \mathcal{E}_T [23], to compute a normalized embedding for the style text:

$$\mathbf{z}_{\text{style}} = \frac{\mathcal{E}_T(t_{\text{style}})}{\|\mathcal{E}_T(t_{\text{style}})\|_2} \quad (1)$$

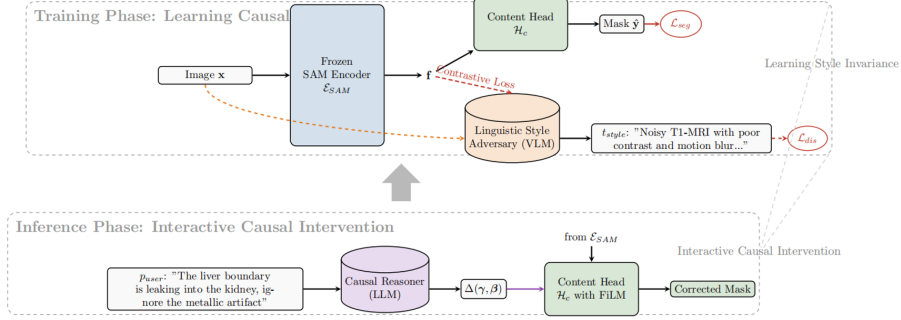


Fig. 1: **The Causal-SAM-LLM Framework. (Top) Training Phase:** A frozen SAM encoder provides features \mathbf{f} . A content head \mathcal{H}_c is trained for segmentation (\mathcal{L}_{seg}). Simultaneously, a frozen VLM acts as a linguistic adversary, generating a rich text description of the image’s style, t_{style} . A contrastive disentanglement loss (\mathcal{L}_{dis}) pushes the image features \mathbf{f} away from the text embedding of t_{style} , forcing the model to learn style-invariant representations. **(Bottom) Inference Phase:** At test time, a user provides a natural language prompt p_{user} describing a segmentation error. A Causal Reasoner (LLM) interprets the prompt and predicts modulation parameters (γ, β) for FiLM layers within the Content Head, producing a corrected segmentation mask.

Simultaneously, the high-dimensional image feature \mathbf{f} from the SAM encoder is passed through a lightweight, trainable projection head, proj_I , which is a Multi-Layer Perceptron (MLP). This maps \mathbf{f} into the same embedding space as the text features, followed by L2 normalization:

$$\mathbf{z}_{\text{image}} = \frac{\text{proj}_I(\mathbf{f})}{\|\text{proj}_I(\mathbf{f})\|_2} \quad (2)$$

The disentanglement loss, \mathcal{L}_{dis} , is then defined to directly quantify and thus enable the minimization of the alignment between these two embeddings. We define it as the cosine similarity, which, for normalized vectors, is their dot product:

$$\mathcal{L}_{dis}(\mathbf{z}_{\text{image}}, \mathbf{z}_{\text{style}}) = \mathbf{z}_{\text{image}} \cdot \mathbf{z}_{\text{style}}^\top \quad (3)$$

This loss term produces a scalar value in $[-1, 1]$. A high value indicates strong alignment between the image features and the style description (the undesirable outcome), while a low or negative value indicates orthogonality or dissimilarity.

The complete training objective combines the primary segmentation loss with this new disentanglement penalty. The model is trained to minimize the following total loss:

$$\mathcal{L}_{\text{total}} = \mathcal{L}_{\text{seg}}(\mathcal{H}_c(\mathbf{f}), \mathbf{y}) + \lambda \mathcal{L}_{dis}(\mathbf{z}_{\text{image}}, \mathbf{z}_{\text{style}}) \quad (4)$$

Here, \mathcal{L}_{seg} is a standard combination of Dice loss and binary cross-entropy. The hyperparameter $\lambda > 0$ controls the strength of the disentanglement penalty.

Table 1: Overview of the datasets used to construct our comprehensive evaluation benchmark. All models are trained exclusively on the BTCV dataset and evaluated across four distinct scenarios: In-Domain (ID), Out-of-Distribution Cross-Scanner (OOD-Scan), Cross-Modality (OOD-Modality), and Cross-Anatomy (OOD-Anatomy).

| Dataset | Anatomy | Scans | Modality | Role in Benchmark |
|-----------------|---------|-------|----------------------------|-------------------------------|
| BTCV [24] | Abdomen | 30 | CT | Training & ID-Test |
| CHAOS [25] | Abdomen | 40 | T1-DUAL MRI T2-SPIR MRI | OOD-Modality |
| AMOS 2022 [4] | Abdomen | 500 | CT | OOD-Scan |
| | | 100 | MRI | OOD-Modality |
| BraTS 2023 [26] | Brain | 1250 | T1ce MRI T2-FLAIR MRI | OOD-Anatomy |

By minimizing the combined objective in Equation 4, the optimization process is forced to find parameters for proj_I and the segmentation head \mathcal{H}_c that not only produce accurate segmentations but also yield image features that are fundamentally decorrelated from their stylistic description. This explicitly steers the model towards a more robust, style-agnostic representation.

3.2 Test-Time Intervention via Causal Reasoning

For interactive correction, we integrate FiLM (Feature-wise Linear Modulation) layers [8] into the decoder, \mathcal{H}_c . A FiLM layer modulates an intermediate feature map \mathbf{h}_i using predicted affine transformation parameters γ_i and β_i : $\text{FiLM}(\mathbf{h}_i) = \gamma_i \odot \mathbf{h}_i + \beta_i$.

At inference, a user provides a natural language prompt p_{user} detailing an observed error. A Causal Reasoner module, \mathcal{R}_{LLM} (a LoRA-finetuned Llama-3-8B model), processes this prompt to predict the full set of FiLM parameters for the decoder:

$$\{\gamma, \beta\} = \mathcal{R}_{LLM}(p_{user}) \quad (5)$$

The reasoner is trained on a synthetically generated dataset mapping error descriptions (e.g., “over-segmentation of the spleen”) to corrective actions (e.g., predict $\gamma < 1$ for specific layers). This allows the user to perform a causal intervention, directly manipulating the model’s behavior to align with their expert knowledge.

4 Experiments and Results

4.1 Datasets and Experimental Setup

We adopt a strict single-source domain generalization protocol to test out-of-distribution (OOD) robustness. All models are trained only on the BTCV CT

Table 2: Quantitative comparison (Dice in % and HD95 in mm). All models are trained **only** on the BTCV CT dataset. We compare against standard architectures, various fine-tuned foundation models, and domain generalization methods. Our method shows superior out-of-distribution (OOD) generalization across all settings. Best results are in **bold**.

| Method | Params (M) | In-Domain | | Out-of-Distribution (OOD) | | | |
|-------------------------------|------------|-------------|-------------|---------------------------|-------------|---------------|-------------|
| | | BTCV CT | | Abdomen (Avg) | | Brain (BraTS) | |
| | | Dice ↑ | HD95 ↓ | Dice ↑ | HD95 ↓ | Dice ↑ | HD95 ↓ |
| <i>Standard Architectures</i> | | | | | | | |
| U-Net [1] | 31.0 | 81.7 | 27.2 | 58.9 | 49.5 | 52.3 | 41.1 |
| nnU-Net [3] | 34.5 | 83.2 | 24.5 | 61.6 | 45.3 | 55.1 | 38.4 |
| <i>Foundation Models</i> | | | | | | | |
| MedNeXt [27] | 28.3 | 83.5 | 23.8 | 64.1 | 42.1 | 58.2 | 35.7 |
| SAM-FT [2] | 635.0 | 85.1 | 19.8 | 72.8 | 31.5 | 68.3 | 25.6 |
| MedSAM-FT [9] | 638.2 | 84.8 | 20.5 | 74.5 | 28.9 | 70.5 | 22.8 |
| SAM-LoRA [6] | 12.5 | 84.6 | 21.1 | 71.8 | 33.8 | 67.2 | 27.9 |
| SAM-VPT [28] | 9.8 | 84.2 | 22.3 | 71.1 | 34.5 | 66.5 | 28.8 |
| <i>Domain Generalization</i> | | | | | | | |
| DANN [10] | 35.1 | 81.8 | 28.3 | 74.1 | 30.1 | 69.5 | 24.1 |
| MixStyle [13] | 34.5 | 82.5 | 26.9 | 73.6 | 31.2 | 70.1 | 23.5 |
| <i>Our Method</i> | | | | | | | |
| Causal-SAM (GRL) | 45.2 | 82.9 | 25.1 | 76.0 | 26.5 | 72.8 | 21.3 |
| Causal-SAM-LLM | 52.8 | 83.5 | 23.4 | 79.5 | 18.9 | 75.7 | 17.6 |

dataset and evaluated directly, without fine-tuning, on a challenging benchmark of three unseen public datasets (CHAOS, AMOS, BraTS) that span different scanners, modalities, and anatomies (details in Table 1). We report the mean Dice Coefficient (DSC) and 95% Hausdorff Distance (HD95), with all metrics averaged over three random seeds for reliability.

4.2 Main Quantitative Results

As shown in Table 2, our **Causal-SAM-LLM** sets a new state-of-the-art in out-of-distribution (OOD) generalization. It consistently achieves the highest Dice scores (79.5% on Abdomen, 75.7% on Brain) and the best Hausdorff Distances (18.9 mm and 17.6 mm respectively) across all OOD scenarios.

This result stands in stark contrast to baseline models. For instance, while the fully fine-tuned SAM-FT achieves the top in-domain Dice score of 85.1%, its performance collapses on OOD tasks, dropping over 12 points on the Abdomen dataset. Standard architectures like nnU-Net suffer an even more severe degradation. Domain generalization methods offer a clear improvement over these baselines but are still significantly outperformed by our causal approach.

Table 3: Test-time intervention study on a curated hard OOD subset (50 cases).

| Configuration | Dice (%) \uparrow HD95 (mm) \downarrow | |
|---------------------------|--------------------------------------------|---------------------------------|
| No Intervention | 71.3 \pm 1.2 | 28.5 \pm 3.4 |
| w/ Language Prompt | 76.5\pm 0.9 | 18.2\pm 2.1 |

4.3 Ablation, Intervention, and Cost Analysis

Ablation Studies. Our ablations in Table 4 validate each component’s contribution. Replacing our linguistic adversary with a simpler GRL-based approach significantly degrades OOD performance (Dice -3.3 pts, HD95 +6.2 mm), while removing the adversary entirely is worse still. This confirms the superiority of semantic-level disentanglement. Furthermore, substituting the SAM backbone with a standard U-Net leads to a performance collapse (59.2 Dice), highlighting the critical role of the pre-trained VFM features.

Crucially, our full framework’s OOD performance is not just superior to external baselines but also to our own strong ablation variant, Causal-SAM (GRL), underscoring the significant impact of linguistic causal guidance. This robustness is further evidenced by a remarkably small generalization gap: our method’s OOD Abdomen Dice (79.5%) is only 3.9 points lower than its in-domain score (83.4%), whereas the SAM-FT baseline suffers a far larger 12.3-point drop. This proves the efficacy of our framework in learning truly robust and generalizable representations.

Test-Time Intervention. The practical utility of our interactive mechanism is demonstrated on a hard subset of 50 OOD cases (Table 3). A single language prompt yields remarkable gains, improving the Dice score by **5.2 points** (from 71.3 to 76.5) and reducing the Hausdorff Distance by **10.3 mm** (from 28.5 to 18.2). This confirms the framework’s value as a human-in-the-loop tool for on-the-fly error correction in challenging scenarios.

Computational Cost. Table 4 also details the computational trade-offs. While our full model has more trainable parameters than SAM-LoRA (52.8M vs. 12.5M), this investment yields a substantial **8.2-point** gain in average OOD Dice score. Crucially, the inference latency remains highly comparable (58.5 ms vs. 56.3 ms), demonstrating that our method adds minimal test-time overhead and is practical for deployment.

4.4 Qualitative and Per-Organ Analysis

Visual and Feature-Space Evidence. Figure 2 provides compelling visual evidence. Visual results on challenging OOD samples underscore our method’s robustness. In both cross-scanner (CT-to-CT) and cross-modality (CT-to-MRI)

Table 4: Ablation study and computational cost analysis. OOD performance is the average over all OOD test sets. Latency is measured on an NVIDIA A100 GPU for a 256×256 image.

| Configuration | Trainable Params (M) | Avg. OOD Perf. | | GFLOPs ↓ | Latency (ms) ↓ |
|---------------------------------------|-------------------------|----------------|----------------|-------------|-------------------|
| | | Dice ↑ | HD95 ↓ | | |
| Causal-SAM-LLM (Full) | 52.8 | 78.1 ± 0.7 | 18.4 ± 1.8 | 35.8 | 58.5 |
| - w/o LAD (GRL only) | 45.2 | 74.8 ± 0.9 | 24.6 ± 2.3 | 35.1 | 55.1 |
| - w/o Any Adversary ($\lambda = 0$) | 42.1 | 71.5 ± 1.1 | 32.1 ± 2.7 | 35.1 | 54.9 |
| - nnU-Net backbone | 36.3 | 59.2 ± 1.8 | 42.7 ± 3.9 | 28.4 | 41.2 |
| <i>For Reference: SAM-LoRA</i> | 12.5 | 69.9 ± 1.4 | 31.6 ± 3.4 | 35.2 | 56.3 |

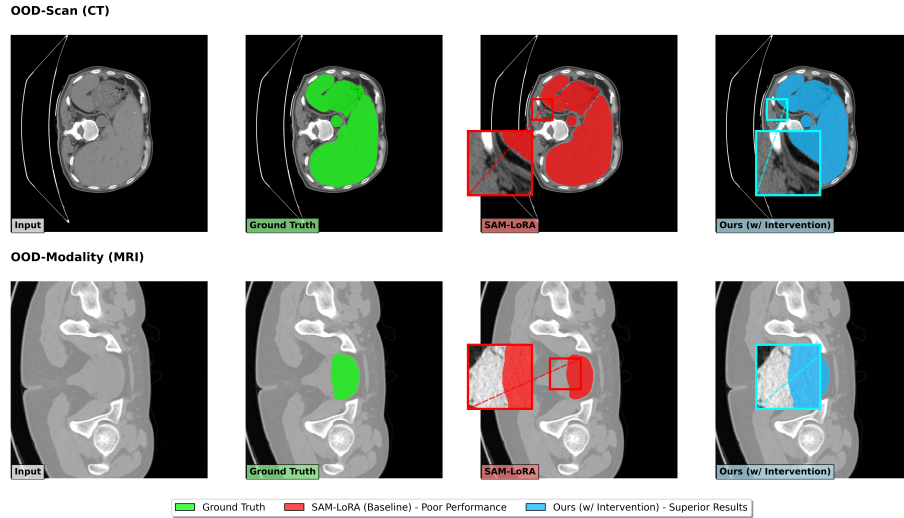
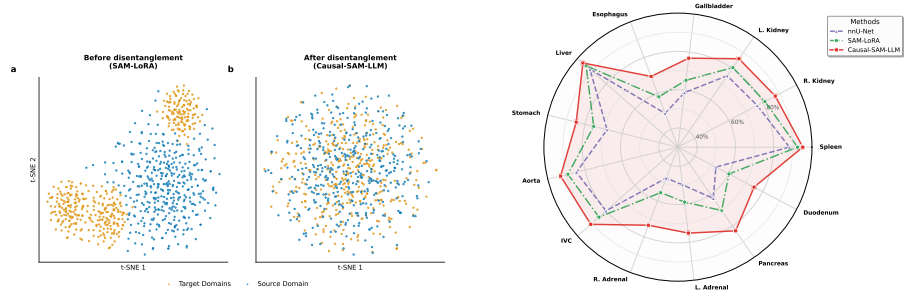


Fig. 2: Qualitative results on challenging OOD samples. Our method is more robust to domain shifts and can be interactively corrected via language prompts to achieve superior accuracy.

settings, baseline models like SAM-LoRA suffer from significant boundary leakage and noisy artifacts. In stark contrast, our Causal-SAM-LLM produces a dramatically cleaner and more accurate initial segmentation, demonstrating its inherent style-agnostic capabilities. Furthermore, the interactive mechanism proves highly effective; a simple natural language prompt enables precise, on-the-fly correction of residual errors, yielding a final mask that aligns closely with the ground truth.

Feature Space Disentanglement. The success of our core mechanism is visually corroborated by the t-SNE embedding of the SAM encoder features (Fig. 3a). The baseline features (a) form distinct, well-separated clusters for the source and



(a) t-SNE visualization of image features, demonstrating successful, language-guided feature space disentanglement.

(b) Per-organ performance analysis on the OOD AMOS CT dataset, showing uniform superiority over baseline methods.

Fig. 3: Feature-space and performance analysis. (a) Our method forces source and target domain features into a single, intertwined cluster. (b) It consistently outperforms baselines across all 13 abdominal organs on an OOD dataset.

target domains, confirming that the representation is entangled with domain-specific style. Conversely, our linguistic adversarial training forces these clusters to collapse into a single, intermingled distribution (b). This provides powerful evidence that our method successfully purges style-related information to learn a truly domain-invariant feature space.

Fine-Grained Performance Breakdown. Finally, the per-organ analysis on the OOD AMOS CT dataset in Figure 3b reveals our method’s uniform superiority. Causal-SAM-LLM (solid red line) consistently forms the outer performance envelope, outperforming both the highly-specialized nnU-Net and the adapted SAM-LoRA across nearly all 13 abdominal organs. The performance uplift is most pronounced on complex structures like the pancreas and adrenal glands, as well as hollow, deformable organs like the stomach and esophagus. This strongly suggests that our model learns true anatomical invariants rather than the brittle, domain-specific shortcuts that limit previous state-of-the-art methods.

5 Conclusion

In this work, we introduced **Causal-SAM-LLM**, a new framework that repurposes Large Language Models as active causal reasoners for medical imaging. By combining proactive, language-guided disentanglement during training with reactive, language-driven intervention at test-time, our method confronts the critical challenge of clinical generalization. Our extensive experiments confirm that this causal approach sets a new state-of-the-art in out-of-distribution robustness. More broadly, our results demonstrate a path beyond pure pattern recognition toward a new class of hybrid AI systems that integrate powerful perceptual backbones with explicit reasoning engines. This not only yields superior

accuracy but also fosters trust by making models directly correctable by human experts, a crucial step for real-world clinical alignment.

References

1. Olaf Ronneberger, Philipp Fischer, and Thomas Brox. U-Net: Convolutional networks for biomedical image segmentation. In *MICCAI*, 2015.
2. Alexander Kirillov, Eric Mintun, Nikhila Ravi, et al. Segment anything. *arXiv preprint arXiv:2304.02643*, 2023.
3. Fabian Isensee, Paul F Jaeger, Simon AA Kohl, Jens Petersen, and Klaus H Maier-Hein. nnU-Net: a self-configuring method for deep learning-based biomedical image segmentation. *Nature Methods*, 18(2):203–211, 2021.
4. Yuanfeng Ji et al. AMOS: A large-scale abdominal multi-organ benchmark for versatile medical image segmentation. *arXiv preprint arXiv:2206.08023*, 2022.
5. Yash Goyal et al. A causal view on robustness of neural networks. *arXiv preprint arXiv:2210.11244*, 2022.
6. Edward J Hu, Yelong Shen, Phillip Wallis, Zeyuan Allen-Zhu, Yanzhi Li, Shean Wang, Lu Wang, and Weizhu Chen. LoRA: Low-rank adaptation of large language models. *arXiv preprint arXiv:2106.09685*, 2021.
7. Chunyuan Li, Cliff Wong, Sheng Zhang, et al. LLaVA-Med: Training a large language-and-vision assistant for biomedicine in one day. *arXiv preprint arXiv:2306.00890*, 2023.
8. Ethan Perez, Florian Strub, Harm De Vries, Vincent Dumoulin, and Aaron Courville. FiLM: Visual reasoning with a general conditioning layer. In *AAAI*, 2018.
9. Jun Ma, , et al. Segment anything in medical images. *arXiv preprint arXiv:2304.12306*, 2023.
10. Yaroslav Ganin, Evgeniya Ustinova, Hana Ajakan, et al. Domain-adversarial training of neural networks. *The Journal of Machine Learning Research*, 17(1):2096–2030, 2016.
11. Haoliang Li, Sinno Jialin Wang, Rui Zhao, and Shiqi He. Domain generalization with mmd-aae. In *Proceedings of the 27th International Joint Conference on Artificial Intelligence*, 2018.
12. Baochen Sun, Jiashi Feng, and Kate Saenko. Return of frustratingly easy domain adaptation. In *AAAI*, 2016.
13. Kaiyang Zhou, Yongxin Yang, Timothy Hospedales, and Tao Xiang. MixStyle: A simple and effective regularization method for domain generalization. In *CVPR*, 2021.
14. Xun Huang and Serge Belongie. Arbitrary style transfer in real-time with adaptive instance normalization. In *Proceedings of the IEEE International Conference on Computer Vision*, 2017.
15. Dequan Wang, Evan Portes, Cédric Paccalin, Oleg Pinykh, et al. Tent: Fully test-time adaptation by entropy minimization. In *International Conference on Learning Representations*, 2021.
16. Judea Pearl. *Causality: Models, Reasoning, and Inference*. Cambridge university press, 2009.
17. Irina Higgins, Loic Matthey, Arka Pal, Christopher Burgess, Xavier Glorot, Matthew Botvinick, Shakir Mohamed, and Alexander Lerchner. beta-vae: Learning basic visual concepts with a constrained variational framework. In *ICLR*, 2017.

18. Francesco Locatello, Stefan Bauer, Mario Lucic, Sylvain Gelly, Bernhard Schölkopf, and Olivier Bachem. Challenging common assumptions in the unsupervised learning of disentangled representations. In *ICML*, 2019.
19. Martin Arjovsky, Léon Bottou, Çağlar Gülçehre, and David Lopez-Paz. Invariant risk minimization. *arXiv preprint arXiv:1907.02893*, 2019.
20. Xin Zhang, Shilin Liu, et al. LISA: Reasoning segmentation via large language models. *arXiv preprint arXiv:2308.00692*, 2023.
21. Xueyan Zou, a Zhai, a Hu, et al. Segment everything everywhere all at once. *NeurIPS*, 2023.
22. Alexey Dosovitskiy, Lucas Beyer, Alexander Kolesnikov, Dirk Weissenborn, Xi-aohua Zhai, Thomas Unterthiner, Mostafa Dehghani, Matthias Minderer, Georg Heigold, Sylvain Gelly, et al. An image is worth 16x16 words: Transformers for image recognition at scale. *ICLR*, 2021.
23. Alec Radford, Jong Wook Kim, Chris Hallacy, Aditya Ramesh, Gabriel Goh, Sandhini Agarwal, Girish Sastry, Amanda Askell, Pamela Mishkin, Jack Clark, et al. Learning transferable visual models from natural language supervision. In *ICML*, 2021.
24. Bennett A Landman et al. MICCAI multi-atlas labeling beyond the cranial vault—workshop and challenge. In *Workshop on Multi-Atlas Labeling...*, 2015.
25. Ali Emre Kavur et al. CHAOS challenge-combined (CT-MR) healthy abdominal organ segmentation. *Medical Image Analysis*, 69:101970, 2021.
26. Spyridon Bakas et al. Advancing the cancer genome atlas glioma mri collections with expert segmentation labels and supporting clinical data. *Scientific data*, 5(1):1–13, 2018.
27. Saikat Roy, , et al. MedNeXt: Transformer-driven scaling of convnets for medical image segmentation. *arXiv preprint arXiv:2303.09975*, 2023.
28. Menglin Jia, Luming Tang, Bor-Chun Chen, Claire Cardie, Serge Belongie, Bharath Hariharan, and Ser-Nam Lim. Visual prompt tuning. *ECCV*, 2022.